EMDFNet: Efficient Multi-scale and Diverse Feature Network for Traffic Sign Detection

Pengyu Li¹, Chenhe Liu¹, Tengfei Li¹, Xinyu Wang¹, Shihui Zhang¹ *, and Dongyang Yu²

Yanshan University, Qinhuangdao City, 066000, Hebei Province, China {202111130221, 202211200217, funlee, zora030}@stumail.ysu.edu.cn, sshhzz@ysu.edu.cn
Beijing Rigour Technology Co.,Ltd. yudongyang2022@gmail.com

Abstract. The detection of small objects, particularly traffic signs, is a critical subtask within object detection and autonomous driving. Despite the notable achievements in previous research, two primary challenges persist. Firstly, the main issue is the singleness of feature extraction. Secondly, the detection process fails to effectively integrate with objects of varying sizes or scales. These issues are also prevalent in generic object detection. Motivated by these challenges, in this paper, we propose a novel object detection network named Efficient Multiscale and Diverse Feature Network (EMDFNet) for traffic sign detection that integrates an Augmented Shortcut Module and an Efficient Hybrid Encoder to address the aforementioned issues simultaneously. Specifically, the Augmented Shortcut Module utilizes multiple branches to integrate various spatial semantic information and channel semantic information, thereby enhancing feature diversity. The Efficient Hybrid Encoder utilizes global feature fusion and local feature interaction based on various features to generate distinctive classification features by integrating feature information in an adaptable manner. Extensive experiments on the Tsinghua-Tencent 100K (TT100K) benchmark and the German Traffic Sign Detection Benchmark (GTSDB) demonstrate that our EMDFNet outperforms other state-of-the-art detectors in performance while retaining the real-time processing capabilities of single-stage models. This substantiates the effectiveness of EMDFNet in detecting small traffic signs.

Keywords: Small object detection \cdot Traffic signs \cdot Multi-scale fusion \cdot Feature diversity.

1 Introduction

Traffic sign detection and recognition (TSD and TSR) are crucial in intelligent transportation and autonomous driving. They aim to detect traffic signs and identify their types for information extraction and safety enhancement. Unlike some studies that separate "detection" (localization) and "recognition" (classification), we consider that TSD includes both in a broader range of object detection.

^{*} Corresponding author: Shihui Zhang, Email: (sshhzz@ysu.edu.cn)
The work is partially supported by the Hebei Natural Science Foundation No.F2023203012.

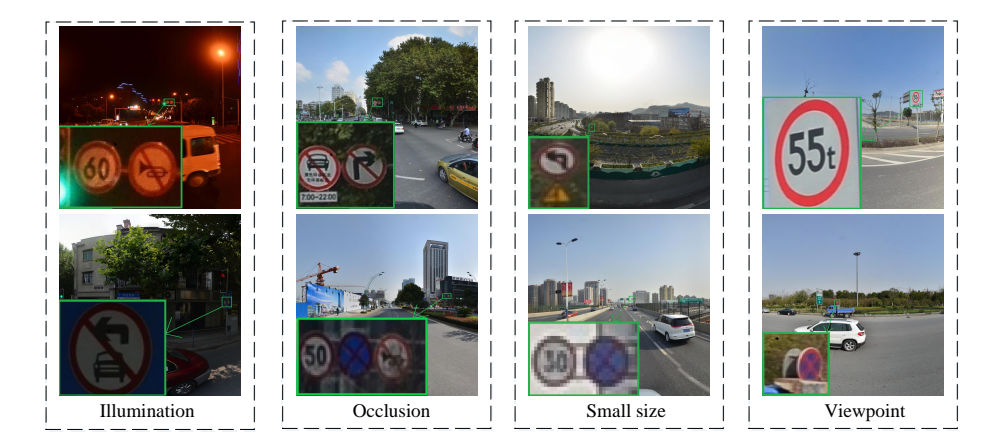


Fig. 1: The difficulties in traffic sign detection. In real traffic scenes, traffic sign detection faces many difficulties including illumination, occlusion, small size, viewpoint and so on.

TSD faces challenges, notably inefficiency due to small sign sizes at long distances, exemplified by signs covering only about 25×25 pixels in 2000×2000 pixel images. The issue of size, combined with the tendency of generic detection models to focus on smaller input resolutions, increases the risk of missing small signs. Additionally, as shown in Fig. 1, detection accuracy is compromised by factors such as complex background, occlusion, deformation, and change in lighting.

Motivated by the above problems, we propose an Efficient Multi-scale and Diverse Feature Network for traffic sign detection in complex background. The contributions of this paper are summerized as four-folds:

- We propose an Efficient Multi-scale and Diverse Feature Network (EMDFNet) for small object detection in complex background. The network possesses a highly powerful capability for feature extraction and multi-scale interaction, thereby enhancing the robustness of small object detection. The network achieves good trade-offs in terms of completeness, real-time processing, and accuracy.
- We propose an Augmented Shortcut Module (ASM) to address the issue of feature singularity. The module combines different spatial semantic information and channel semantic information through multiple branches to enhance feature diversity. Our ASM excels at capturing the fundamental visual patterns and semantic information of small objects, thereby enhancing the effectiveness of small object detection.
- To enhance multi-scale detection capability of the network, we introduce the Efficient Hybrid Encoder (EHE) to improve the neck structure. This encoder combines intra-scale feature interaction and cross-scale feature fusion. To the best of our knowledge, we are the first to apply the idea of EHE to the field of traffic sign detection.
- Extensive experiments are conducted on two widely used datasets TT100K and GTSDB. The experimental results in both qualitative and quantitative dimensions demonstrate that the proposed EMDFNet reliably achieves state-of-the-art performance in traffic sign detection.

2 Related Work

2.1 Object Detection

Deep convolutional neural networks (CNNs) have become the preferred choice for various computer vision tasks in recent years. They have significantly improved the accuracy and speed of object detection, as evidenced in benchmarks such as Pascal VOC [1] and MS COCO [2]. The R-CNN series, including R-CNN [3], Fast R-CNN [4], Faster R-CNN [5], and Mask R-CNN [6], extract region proposals before classifying and regressing them for detection results. However, their two-stage process is computationally intensive, limiting their practical use. Single-stage detectors like SSD [7] and YOLO eliminate the proposal step to enable real-time performance but face challenges with small objects because of the loss of spatial and channel details. This paper aims to preserve spatial and channel feature information to enhance the detection performance of small traffic signs.

2.2 Traffic Sign Detection

Traffic sign detection (TSD) is a specialized area within object detection, where generic methods are less effective due to the small size and complex detection requirements of traffic signs. Traditional techniques focus on handcrafted features such as color, shape, and edges, often combined with machine learning classifiers. However, these methods struggle with environmental variations such as lighting and motion blur.

Recent advancements have seen the rise of CNN-based approaches, utilizing strategies such as fully convolutional networks (FCN) [8] for sign proposals and deep CNNs for classification. Additionally, techniques involving image pyramids and Generative Adversarial Networks (GANs) have been employed to enhance detection performance, particularly for small objects. Despite successes, limitations remain in data availability and sign size, impacting the balance between speed, accuracy, and detection completeness. This paper focuses on the trade-off between accuracy and speed.

3 Proposed Network

3.1 Network Overview

As illustrated in Fig. 2, our EMDFNet, an end-to-end object detection network that incorporates multi-scale feature fusion and diverse features. EMDFNet leverages Res2Net [9] as the backbone to extract three feature maps. The feature map with the largest receptive field is first fed into the Augmented Shortcut Module (ASM). Subsequently, the feature map processed by ASM and the other two feature maps are input into the Efficient Hybrid Encoder (EHE). The ASM enhances feature representation and preserves details, while the EHE achieves better cross-scale fusion. Ultimately, the network integrates three detection heads to obtain detection results after classification and regression tasks.

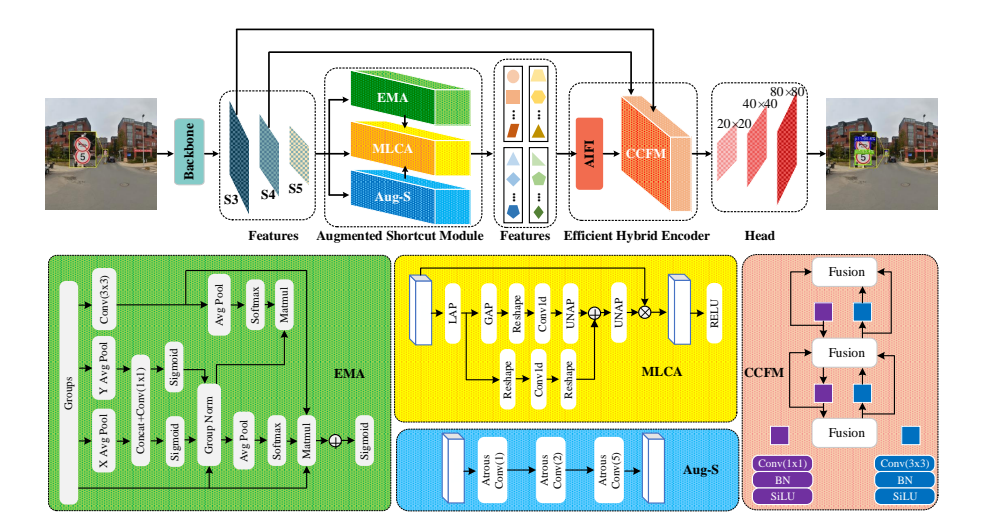


Fig. 2: The EMDFNet can be roughly divided into four parts. The first part consists of a backbone composed of Res2Net. The second part is the Augmented Shortcut Module, which enhances feature diversity. The third part is the Efficient Hybrid Encoder for integrating multi-scale features. Finally, the fourth part comprises three prediction heads for bounding box prediction.

3.2 Augmented Shortcut Module

To address the issue of too single features extracted by the backbone, we propose a powerful Augmented Shortcut Module (ASM) to increase feature diversity in our EMDFNet through refining shortcut connections. ASM includes spatial feature selection, channel feature selection and Aug-S. The module parallelizes three branches and then outputs diversified features. The final structure of the ASM is shown in Fig. 2. The ASM can be formulated as follows:

$$ASM = MLCA(\Gamma(Z_l, \Theta_l), shortcut(Z_l), FS(Z_l))$$
(1)

The augmented shortcut connection, denoted as Γ with parameters Θ , enhances the original shortcut by adding alternative paths that incorporate attention mechanisms. Unlike simple identity projection, Γ transforms input features into a new space using various transformations dictated by Θ . The feature selection (FS) utilizes Efficient Multi-scale Attention (EMA) [10] to select spatial features, and all branches undergo processing by the Mixed Local Channel Attention (MLCA) [11] channel selection module before concatenation.

The original residual connection is updated with two main components: a feature selection layer for spatial and channel features, and an enhanced shortcut connection Aug-S. We utilize spatial feature selection to uniformly distribute spatial semantics and utilize channel feature selection to fuse local and global channel information. In addi-

tion, Aug-S consists of a set of dilated convolutions that expand the receptive field while keeping the image size unchanged. Aug-S enhances feature diversity as an alternative route. To preserve details lost during downsampling by the backbone, we utilize Hybrid Dilated Convolution (HDC) with dilation rates of [1,2,5]. This approach helps avoid the gridding effect associated with uniform dilation rates and ensuring comprehensive pixel utilization. As shown in Fig. 3. This approach improves the retention of feature map details.

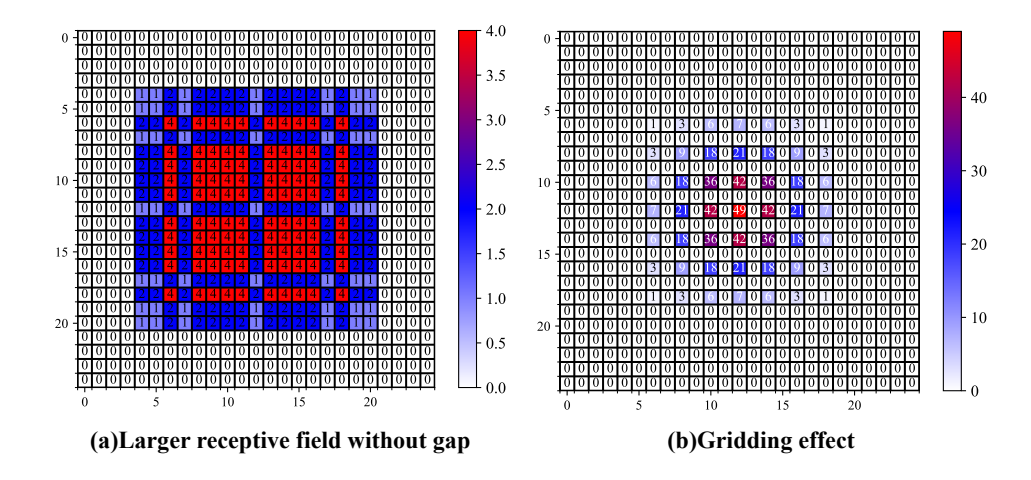


Fig. 3: The dilation rates used in (a) are [1, 2, 5], where all pixel values are effectively utilized, while in (b), the dilation rates are [2, 2, 2], resulting in a gridding effect.

3.3 Efficient Hybrid Encoder

To enhance the multi-scale fusion capability of the proposed EMDFNet, we introduce the Efficient Hybrid Encoder (EHE) for the first time in the field of traffic sign detection, as illustrated in Fig. 2. EHE is an excellent component accepted in CVPR 2024, which can achieve multi-scale fusion through intra-scale interaction and cross-scale interaction [12]. EHE comprises two main units: an Attention-based Intrascale Feature Interaction (AIFI) for reducing computational redundancy by emphasizing high-level intra-scale interactions, and a CNN-based Cross-scale Feature-fusion Module (CCFM), which introduces fusion blocks to combine adjacent feature levels. As shown in formula 2, AIFI prioritizes high-level features for their richer semantic content, avoiding lower-level interactions that could lead to duplication or confusion. As shown in formula 3, CCFM's fusion blocks, combine features through element-wise addition, optimizing feature integration to enhance object detection and recognition performance.

$$F_5 = AIFI(S_5) \tag{2}$$

Output =
$$\operatorname{CCFM}(\{S_3, S_4, F_5\})$$
 (3)

where S3, S4, S5, F5 are feature maps. AIFI first decomposes the feature map into sequence vectors, and then resynthesizes the feature map through the attention mechanism. CCFM fuses feature maps of different sizes.

3.4 Loss Function

IoU Loss has several limitations, including its inability to optimize when boxes do not intersect (IoU=0), its failure to indicate the distance between boxes, and its inaccuracy in showing the degree of overlap. To overcome IoU Loss limitations, we introduce SIoU Loss [13] for calculating rectangular box loss, enhancing training speed and detection precision.

The SIoU Loss function is defined as follows:

$$L_{box} = 1 - IoU + \frac{L_{dis} + L_{shape}}{2} \tag{4}$$

$$L = W_{box}L_{box} + W_{cls}L_{cls} \tag{5}$$

where L_{box} represents shape cost. IoU (Intersection over Union) represents the intersection of the union loss. L_{dis} and L_{shape} represent the distance cost and the shape loss, respectively. W_{box} and W_{cls} represent weights assigned to the bounding box and classification losses, respectively. L_{cls} represents the focal loss. From these we can obtain the final loss function L.

4 Experiment

4.1 Dataset

We use the TT100K and GTSDB datasets to evaluate our EMDFNet.

- TT100K [14] provides 1,000,000 images and 30,000 annotated traffic signs that are collected from Tencent Street Views in Chinese Cities. The resolution of the provided images is uniform 2048 × 2048 pixels. We ignore categories with fewer than 100 instances following, thus leaving 45 categories to detect, as illustrated in Fig. 4. The publicly available benchmark dataset can be found at http://cg.cs.tsinghua.edu.cn/traffic-sign/. To avoid the impact of various augmentation policies, we fine-tune the proposed EMDFNet and other detectors on the original training set, which includes 6105 images, and test them on the original testing set, which comprises 3071 images, for a fair comparison. Three categories labeled as 'ph5', 'w32', and 'wo' are excluded due to their mixed content of several traffic signs.
- GTSDB [15] provides 900 images and 1213 annotated traffic signs. All these images are captured from video sequences recorded near Bochum, Germany. The benchmark dataset is publicly available at https://benchmark.ini.rub.de/gtsdb_dataset.html. The final images are clipped to 1360×800 pixels. The standard task for GTSDB focuses on traffic signs, and all traffic signs are classified into four major categories: prohibitory, danger, mandatory, and other.



Fig. 4: Illustrations of 45 remaining traffic sign categories from the TT100K dataset.

4.2 Implementation Details

We develop EMDFNet using PyTorch 1.8.0 on an RTX 3090 GPU, utilizing pretrained Res2Net-101 weights to expedite training. Our batch size is 8 for 640×640 inputs, dropping to 4 for 1024×1024 inputs due to memory constraints. We apply multi-scale inputs, mosaics, and mixup augmentations for better generalization. Training involves 400 epochs on the TT100K dataset and 100 epochs on the GTSDB dataset, starting with a five-epoch warm-up at a zero learning rate. We utilize Stochastic Gradient Descent (SGD) with a weight decay of 0.0005 and momentum of 0.9. The learning rate is adjusted using linear warm-up and cosine annealing techniques, customizing for each stage of training.

4.3 Evaluation Metrics

To assess network performance, we utilize Average Precision (AP), parameters, GFLOPs, and Frames Per Second (FPS) as metrics.

Average Precision (AP) is an evaluation index of detection accuracy, calculated as the average value of the average accuracy across multiple categories. AP is defined as the area under the curve, which depends on recall and accuracy. The function to calculate AP is shown below formula 6. P(R) is the curve based on the recall rate and precision rate. Mean Average Precision (mAP) is a comprehensive criterion that is shown below formula 7. N is the number of categories in the function.

$$AP = \int_0^1 P(R)dR \tag{6}$$

$$mAP@IoU = \frac{1}{N} \sum_{i=1}^{N} AP@IoU$$
(7)

mAP@.5 represents the model's accuracy in object detection with a minimum 50% overlap between predicted and actual bounding boxes. mAP@.75 evaluates precision

with a stricter 75% overlap requirement. mAP@.5:.95 averages mAP over IoU thresholds from 0.5 to 0.95. It provides a comprehensive overview of the model's performance across a range of criteria from lenient to strict. In object detection, AP_s , AP_m , and AP_l represent average precision metrics calculated for objects of small, medium, and large sizes detected within images.

Parameters calculate the number of parameter in the model, indicating memory resource usage. GFLOPs measure computational complexity as billions of operations per second. FPS, the rate of image processing, reflects real-time performance and is affected by image resolution. Higher resolutions reduce FPS with the same model and conditions.

4.4 Quantitative Analysis

Comparisons of SOTA on TT100K Dataset. We compare the proposed approach with state-of-the-art traffic sign detection methods. Table 1 presents the mAP@.5, mAP@.75, mAP@.5:.95, AP_s , AP_m , and AP_l values of the proposed method compared to other well-known detectors on the TT100K testing dataset. It can be observed that EMDFNet (640) and EMDFNet (1024) achieve 84.4% mAP@.5 and 93.3% mAP@.5, respectively.

From Table 1, we can know when input sizes are similar, EMDFNet significantly outperforms other models. At an input size of 640, it achieves 84.4%, surpassing SSD (68.7%), ScratchDet (74.0%), CAB Net (78.0%), and Open-TransMind (83.0%). At an input size of 1024, EMDFNet achieves 93.3% accuracy. A 23.8% increase over Sparse R-CNN's 69.5%, surpassing Mask R-CNN (70.8%), Faster R-CNN (74.1%), and Cascade R-CNN (80.1%), setting a new benchmark in object detection.

EMDFNet outperforms models with larger inputs, reaching 84.4% mAP@.5 at an input size of 640. This surpasses RetinaNet (61.9%, 2048 input), Sparse R-CNN (69.5%, 1024 input), Faster R-CNN (74.1%, 1024 input), and Cascade R-CNN (80.1%, 1024 input). Despite using smaller inputs, EMDFNet significantly enhances mAP, demonstrating its exceptional efficiency.

It can be seen from Table 1 that our network focuses on detecting small and medium traffic signs, with a particular emphasis on AP_s . Sparse R-CNN, Faster R-CNN, Cascade R-CNN, and SwinT + Cascade R-CNN achieve AP_s of 35.6%, 27.7%, 36.2%, and 44.5%, respectively. EMDFNet achieves 55.4% and 61.1% AP_s at input sizes of 640 and 1024, respectively, demonstrating its effectiveness in detecting smaller objects.

To further verify the performance of the proposed network, Table 2 shows the detection accuracy of EMDFNet in each category and compares it with other networks. From the Table 2 we can see that EMDFNet achieves SOTA in almost all categories. In particular, the accuracy of 'p27' reach 100.0%, 'il60' reach 99.8%, and 'il80' reach 98.9%.

In summary, it can be concluded that our EMDFNet's efficacy is clear: Res2Net enhances feature extraction, Augmented Shortcut Module diversifies input features, and Efficient Hybrid Encoder enhances multi-scale integration, thereby enhancing small traffic sign detection. Additionally, larger input sizes yield higher AP_s , indicating the potential for further enhancements in small object detection performance.

Table 1: The performance of different models on the TT100K dataset. The best results are shown in bold.

Model	Year	Input Size	mAP@.5	mAP@.75	mAP@.5:.95	AP_s	AP_m	AP_l	FPS	Param.	GFLOPS
Faster R-CNN [5]	2015	1024×1024	74.1	69.3	58.9	27.7	73.1	81.8	21	41.6	211.5
SSD512 [7]	2016	512 × 512	68.7	-	-	-	-	-	-	-	-
TT100K [14]	2016	640×640	83.3	79.0	65.8	-	-	-	-	35.1	-
RetinaNet [16]	2017	2048×2048	61.9	-	-	-	-	-	-	-	-
Mask R-CNN [6]	2017	1000×800	70.8	-	-	-	-	-	-	-	-
Cascade-RCNN [17]	2018	1024×1024	80.1	74.8	63.5	36.2	74.6	83.0	17.0	69.3	239.2
ScratchDet [18]	2019	512 × 512	74.0	-	-	-	-	-	-	-	-
FCOS [19]	2019	2048×2048	83.3	-	-	-	-	-	-	-	-
PCN [20]	2020	2048×2048	92.0	86.6	72.1	-	-	-	-	34.3	-
Sparse R-CNN [21]	2021	1024×1024	69.5	62.8	53.2	35.6	61.2	70.6	21.0	106.2	153.3
Swint-T+Cascade R-CNN [22]	2021	1024×1024	86.3	79.1	68.6	44.5	73.7	85.2	14.0	74.6	245.5
CAB Net [23]	2022	512 × 512	78.0	-	-	-	-	-	-	-	-
TRD-YOLO [24]	2023	640 × 640	37 .5	-	30.1	26.8	34.5	40.2	-	-	-
YOLO-SG [25]	2023	640×640	75.8	-	-	-	-	60.2	-	-	
Open-TransMind [26]	2023	512 × 512	83.0	-	-	-	-	-	-	-	-
Transformer Fusion [27]	2024	640×640	53.5	-	39.5	43.6	43.7	58.6	-	-	-
EMDFNet(ours)	-	640 × 640	84.4	76.8	64.9	55.4	68.5	81.7	46.7	29.7	98.4
EMDFNet(ours)	-	1024 × 1024	93.3	87.1	73.8	61.1	78.8	85.4	31.0	29.6	187.8

Comparisons of SOTA on GTSDB Dataset. To further verify the performance of our EMDFNet, we conduct experiments based on the GTSDB dataset. We fix the input size of the model to match the original image size of the dataset for comparison under consistent condition. The experimental results are shown in Table 3. From Table 3, we can observe that under the same input condition, the mAP@.5 value of EMDFNet reach 97.0%, significantly surpassing the performance of other models. Among them, the most notable improvement is that EMDFNet is 35.4% higher than SSD Mobilenet (from 61.6% to 97.0%).

When compared with Faster R-CNN Inception ResNet V2, the increase in mAP@.5 value is significant (from 95.7% to 97.0%), and the FPS of EMDFNet is about eight times higher, with a significant reduction in the number of parameters and computational cost. This demonstrates that EMDFNet not only performs well in accuracy but also achieves good results in speed and real-time performance.

Through comparisons of different datasets (TT100K and GTSDB), it is found that EMDFNet consistently achieves state-of-the-art performance levels, indicating that EMDFNet demonstrates excellent generalization capability.

Analyzing Object Detection Errors. We compare EMDFNet and YOLOX using the TIDE toolkit to tabulate error distributions on the TT100K testing set, as presented in Table 4. EMDFNet exhibites a lower classification error than YOLOX (10.02% vs. 11.22%), attributed to the Augmented Shortcut Module enhancing feature diversity and Efficient Hybrid Encoder improving feature spatial distribution for classification. EMDFNet also demonstrates a decreased miss error rate (0.98% vs. 1.87%), attributed to its effective feature extraction, which reduces the omission of essential details, thereby enhancing localization and classification accuracy. Both and Dupe are basically the same, which may be caused by dataset noise. The remaining error rates decrease.

Table 2: Comparisons of AP for each category on the TT100K testing set. Each column represents a traffic sign. The EMDFNet outperforms other detectors, achieving the SOTA performance.

Method 12 14 15 1100 1160 180 10 10 10 10 10 11 11	301A periorman	cc.													
Faster R-CNN [28] 59.3 73.8 79.7 76.6 76.3 68.5 64.9 66.8 52.2 58.5 45.9 48.2 74.4 66.1 FPN [29] 72.5 79.6 88.3 90.2 88.2 84.9 77.4 75.8 62.7 75.9 60.2 53.7 75.8 76.0 Mask R-CNN [6] 71.4 85.6 89.0 89.4 86.3 82.3 78.0 77.6 59.6 76.9 63.8 52.0 72.9 81.7 SSD512 [7] 70.1 79.3 85.3 77.1 86.4 78.7 72.3 71.6 64.5 57.1 67.7 73.0 80.4 70.7 DSSD512 [30] 65.0 86.2 88.6 62.7 87.7 76.2 60.2 85.5 66.2 55.1 54.4 78.4 79.3 75.5 RFB Net 512 [31] 75.6 79.4 87.9 87.4 89.9 88.4 77.2 79.0 66.1 66.9 71.1 72.8 83.4 74.9 ScratchDet [18] 76.0 87.5 89.4 80.6 89.9 85.3 80.5 78.0 69.1 77.6 74.3 87.6 87.1 81.4 CAB-s Net [23] 75.2 86.4 89.4 84.9 89.2 89.1 81.6 77.8 69.7 72.4 72.3 89.0 88.3 81.6 EMDFNet(ours) 84.0 93.5 96.1 95.1 99.8 98.9 84.6 86.9 81.8 89.9 85.8 81.5 89.9 87.6 EMDFNet(ours) 84.0 93.5 96.1 95.1 99.8 98.9 84.6 86.9 81.8 89.9 85.8 81.5 89.9 87.6 EMDFNet(ours) 78.5 78.9 48.3 88.5 63.9 58.1 86.7 86.5 55.7 55.6 71.5 77.3 60.8 58.7 60.2 66.5 74.9 63.9 84.2 62.1 51.2 81.8 84.9 85.8 86.2 66.2 65.4 49.0 51.2 FPN [29] 71.6 79.2 39.1 78.2 58.0 36.5 87.5 85.5 55.7 55.6 71.5 77.3 60.8 58.7 66.5 74.9 63.9 84.2 62.1 51.2 85.1 84.2 45.4 66.6 65.7 60.5 58.3 64.0 64.8 64.	Method	i2	i4	i5	il100	il60	i180	io	ip	p10	p11	p12	p19	p23	p26
FPN [29] 72.5 79.6	Faster R-CNN [5]	44.0	46.0	45.0	41.0	57.0	62.0	41.0	39.0	45.0	38.0	60.0	59.0	65.0	50.0
Mask R-CNN [6]	Faster R-CNN [28]	59.3	73.8	79.7	76.6	76.3	68.5	64.9	66.8	52.2	58.5	45.9	48.2	74.4	66.1
SSD512 [7]	FPN [29]	72.5	79.6	88.3	90.2	88.2	84.9	77.4	75.8	62.7	75.9	60.2	53.7	75.8	76.0
DSSD512 [30] 65.0 86.2 88.6 62.7 87.7 76.2 60.2 85.5 66.2 55.1 54.4 78.4 79.3 75.5	Mask R-CNN [6]	71.4	85.6	89.0	89.4	86.3	82.3	78.0	77.6	59.6	76.9	63.8	52.0	72.9	81.7
RFB Net 512 [31] 75.6 79.4 87.9 87.4 89.9 88.4 77.2 79.0 66.1 66.9 71.1 72.8 83.4 74.9 ScratchDet [18] 76.6 86.9 89.2 82.2 88.8 81.3 73.9 77.3 68.8 65.3 70.8 67.2 80.2 74.9 CAB Net [23] 76.0 87.5 89.4 80.6 89.9 85.3 80.5 78.0 69.1 77.6 74.3 87.6 87.1 81.4 CAB-s Net [23] 75.2 86.4 89.4 84.9 89.2 89.1 81.6 77.8 69.7 72.4 72.3 89.0 88.3 81.6 EMDFNet(ours) 84.0 93.5 96.1 95.1 99.8 98.9 84.6 86.9 81.8 89.9 85.8 81.5 89.0 88.3 81.6 EMDFNet(ours) 84.0 93.5 96.1 95.1 99.8 98.9 84.6 86.9 81.8 89.9 85.8 81.5 89.0 88.3 81.6 EMDFNet(ours) 84.0 93.5 96.1 95.1 99.8 98.9 84.6 86.9 81.20 pl30 pl40 pl5 pl50 pl50 pl50 pl50 Faster R-CNN [5] 48.0 77.0 75.0 80.0 5.0 67.0 76.0 <td>SSD512 [7]</td> <td>70.1</td> <td>79.3</td> <td>85.3</td> <td>77.1</td> <td>86.4</td> <td>78.7</td> <td>72.3</td> <td>71.6</td> <td>64.5</td> <td>57.1</td> <td>67.7</td> <td>73.0</td> <td>80.4</td> <td>70.7</td>	SSD512 [7]	70.1	79.3	85.3	77.1	86.4	78.7	72.3	71.6	64.5	57.1	67.7	73.0	80.4	70.7
ScratchDet [18] 76.6 86.9 89.2 82.2 88.8 81.3 73.9 77.3 68.8 65.3 70.8 67.2 80.2 74.9 CAB Net [23] 76.0 87.5 89.4 80.6 89.9 85.3 80.5 78.0 69.1 77.6 74.3 87.6 87.1 81.4 EMDFNet(ours) 84.0 93.5 96.1 95.1 99.8 98.9 84.6 86.9 81.8 89.9 85.8 81.5 89.9 87.6 Method p3 p5 p6 pg ph4 ph4.5 pl100 pl120 pl20 pl30 pl40 pl5 pl50 pl60 Faster R-CNN [5] 48.0 57.0 75.0 80.0 68.0 58.0 68.0 67.0 51.0 43.0 52.0 53.0 39.0 53.0 Faster R-CNN [28] 65.4 74.9 39.1 78.2 58.0 36.5 77.6 74.6 40.5 48.5 60.2 65.4 49.0 51.2 FPN [29] 71.6 79.2 39.1 78.2 58.0 36.5 77.6 74.6 40.5 48.5 60.2 65.4 49.0 51.2 FRN [29] 71.6 65.7 49.3 88.2 63.0 36.1 <td< td=""><td>DSSD512 [30]</td><td>65.0</td><td>86.2</td><td>88.6</td><td>62.7</td><td>87.7</td><td>76.2</td><td>60.2</td><td>85.5</td><td>66.2</td><td>55.1</td><td>54.4</td><td>78.4</td><td>79.3</td><td>75.5</td></td<>	DSSD512 [30]	65.0	86.2	88.6	62.7	87.7	76.2	60.2	85.5	66.2	55.1	54.4	78.4	79.3	75.5
CAB Net [23] 76.0 87.5 89.4 80.6 89.9 85.3 80.5 78.0 69.1 77.6 74.3 87.6 87.1 81.4 CAB-s Net [23] 75.2 86.4 89.4 84.9 89.2 89.1 81.6 77.8 69.7 72.4 72.3 89.0 88.3 81.6 EMDFNet(ours) 84.0 93.5 96.1 95.1 99.8 98.9 84.6 86.9 81.8 89.9 85.8 81.5 89.9 87.6 Method p3 p5 p6 pg ph4 ph4.5 pl100 pl120 pl20 pl20 pl30 pl40 pl5 pl50 pl50 pl60 Faster R-CNN [5] 48.0 57.0 75.0 80.0 68.0 58.0 68.0 67.0 51.0 43.0 52.0 53.0 39.0 53.0 Faster R-CNN [6] 78.5 74.9 39.1 78.2 58.0 36.5 77.6 74.6 40.5 48.5 60.2 65.4 49.0 51.2 FPN [29] 71.6 79.2 39.1 78.2 58.0 36.5 87.5 85.5 55.7 55.6 71.5 77.3 60.8 58.7 Mask R-CNN [6] 78.5 78.9 48.3 88.5 63.9 58.1 86.7 82.4 58.6 53.3 68.2 61.5 65.4 69.0 75.6 65.1 <td>RFB Net 512 [31]</td> <td>75.6</td> <td>79.4</td> <td>87.9</td> <td>87.4</td> <td>89.9</td> <td>88.4</td> <td>77.2</td> <td>79.0</td> <td>66.1</td> <td>66.9</td> <td>71.1</td> <td>72.8</td> <td>83.4</td> <td>74.9</td>	RFB Net 512 [31]	75.6	79.4	87.9	87.4	89.9	88.4	77.2	79.0	66.1	66.9	71.1	72.8	83.4	74.9
CAB-s Net [23] 75.2 86.4 89.4 84.9 89.2 89.1 81.6 77.8 69.7 72.4 72.3 89.0 88.3 81.6 EMDFNet(ours) 84.0 93.5 96.1 95.1 99.8 98.9 84.6 86.9 81.8 89.9 85.8 81.5 89.9 87.6 Method p3 p5 p6 pg ph4 ph4.5 ph100 pl120 pl20 pl30 pl40 pl5 pl50 pl50 pl50 pl60 Faster R-CNN [5] 48.0 57.0 75.0 80.0 68.0 58.0 68.0 67.0 51.0 43.0 52.0 53.0 39.0 53.0 Faster R-CNN [28] 65.4 74.9 39.1 78.2 58.0 36.5 77.6 74.6 40.5 48.5 60.2 65.4 49.0 51.2 FPN [29] 71.6 79.2 39.1 78.2 58.0 36.5 87.5 85.5 55.7 55.6 71.5 77.3 60.8 58.7 Mask R-CNN [6] 78.5 78.9 48.3 88.5 63.9 58.1 86.7 82.4 58.6 53.3 68.2 76.4 63.5 56.6 SSD512 [7] 66.5 74.9 63.9 84.2 62.1 51.2 85.1 84.2 45.4 66.6 65.7 60.5 58.3 64.0 DSSD512 [30] 76.1 79.6	ScratchDet [18]	76.6	86.9	89.2	82.2	88.8	81.3	73.9	77.3	68.8	65.3	70.8	67.2	80.2	74.9
EMDFNet(ours) 84.0 93.5 96.1 95.1 99.8 98.9 84.6 86.9 81.8 89.9 85.8 81.5 89.9 87.6 Method p3 p5 p6 pg ph4 ph4.5 pl100 pl20 pl30 pl40 pl5 pl60 Faster R-CNN [5] 48.0 57.0 75.0 80.0 68.0 58.0 68.0 67.0 51.0 43.0 52.0 53.0 39.0 53.0 Faster R-CNN [28] 65.4 74.9 39.1 78.2 58.0 36.5 77.6 74.6 40.5 48.5 60.2 65.4 49.0 51.2 FPN [29] 71.6 79.2 39.1 78.2 58.0 36.5 87.5 85.5 55.7 55.6 71.5 77.3 60.8 88.7 Mask R-CNN [6] 78.5 78.9 48.3 88.5 63.9 58.1 86.7 82.4 58.6 53.3 68.2 76.4 49.0 56.6 SSD512 [7] 66.5 74.9 63.9 84.2 62.1 51.2 85.1 84.2 45.4 66.6 65.7 60.5 58.3 64.0 DSSD512 [7] 66.5 74.9 63.9 84.2 62.1 51.2 85.1 84.2	CAB Net [23]	76.0	87.5	89.4	80.6	89.9	85.3	80.5	78.0	69.1	77.6	74.3	87.6	87.1	81.4
Method p3 p5 p6 pg ph4 ph4.5 pl100 pl20 pl30 pl40 pl50 pl60 Faster R-CNN [5] 48.0 57.0 75.0 80.0 68.0 58.0 68.0 67.0 51.0 43.0 52.0 53.0 39.0 53.0 Faster R-CNN [28] 65.4 74.9 39.1 78.2 58.0 36.5 77.6 74.6 40.5 48.5 60.2 65.4 49.0 51.2 FPN [29] 71.6 79.2 39.1 78.2 58.0 36.5 87.5 85.5 55.7 55.6 71.5 77.3 60.8 88.7 Mask R-CNN [6] 78.5 74.9 63.9 84.2 62.1 51.2 85.1 86.7 85.4 58.6 63.3 68.2 61.5 65.5 66.7 SDSD512 [30] 56.1 79.6 55.4 85.8 60.7 88.6 79.1 66.8 78.8 84.7 66.6	CAB-s Net [23]	75.2	86.4	89.4	84.9	89.2	89.1	81.6	77.8	69.7	72.4	72.3	89.0	88.3	81.6
Faster R-CNN [5]	EMDFNet(ours)	84.0	93.5	96.1	95.1	99.8	98.9	84.6	86.9	81.8	89.9	85.8	81.5	89.9	87.6
Faster R-CNN [5]	Method	p3	р5	р6	pg	ph4	ph4.5	pl100	pl120	pl20	pl30	pl40	pl5	pl50	pl60
Faster R-CNN [28] 65.4 74.9 39.1 78.2 58.0 36.5 77.6 74.6 40.5 48.5 60.2 65.4 49.0 51.2 FPN [29] 71.6 79.2 39.1 78.2 58.0 36.5 87.5 85.5 55.7 55.6 71.5 77.3 60.8 58.7 Mask R-CNN [6] 78.5 78.9 48.3 88.5 63.9 58.1 86.7 82.4 58.6 53.3 68.2 76.4 63.5 56.6 SSD512 [7] 66.5 74.9 63.9 84.2 62.1 51.2 85.1 84.2 45.4 66.6 65.7 60.5 58.3 64.0 DSSD512 [30] 56.1 79.6 55.4 85.8 60.7 88.6 79.1 69.6 65.3 68.3 68.2 61.5 65.5 64.7 RFB Net 512 [31] 69.0 77.6 68.8 88.9 67.6 63.0 88.8 84.9 66.8 71.8 71.6 75.0 62.9 70.4 ScratchDet [18] 71.2 87.3 65.4 79.1 66.8 55.7 85.8 84.7 63.6 67.1 73.2 65.4 69.9 72.8 CAB Net [23] 74.7 84.5 82.5 87.5 71.8 64.4 88.4 87.9 68.6 73.3 74.8 79.3 75.1 76.3 CAB-s Net [23] 76.8 85.4 78.0 86.4 71.7 62.3 89.2 88.7 71.5 73.5 75.3 75.9 73.1 75.9 EMDFNet(ours) 88.0 93.6 82.9 94.9 63.2 88.8 92.5 91.6 78.0 80.0 85.0 89.2 84.1 75.3 Method Pl80 pm20 pm30 pm55 pn pne po pr40 w13 w55 w57 w59 p27 pl70 Faster R-CNN [5] 52.0 61.0 67.0 61.0 37.0 47.0 37.0 75.0 33.0 39.0 48.0 39.0 79.0 61.0 Faster R-CNN [6] 70.5 59.0 50.5 29.1 68.5 77.8 87.5 47.7 86.9 30.9 62.1 67.0 57.2 64.3 61.2 FPN [29] 70.9 55.5 40.1 75.7 89.0 89.8 60.2 87.6 45.3 65.9 70.3 62.3 84.8 63.5 Mask R-CNN [6] 71.5 58.0 41.5 68.8 88.6 90.5 63.0 87.5 51.3 66.6 71.1 61.8 87.5 66.3 SD512 [7] 70.5 69.6 51.3 71.2 71.7 86.4 51.8 87.9 46.1 64.6 74.0 58.8 76.2 70.6 SD512 [30] RFB Net 512 [31] 71.9 73.7 54.0 86.5 78.0 88.2 59.8 84.5 64.8 72.4 81.5 69.3 79.8 64.9 SCTACHDet [18] 75.9 73.3 52.2 76.5 76.7 89.4 62.9 85.0 69.1 70.3 84.7 76.5 79.7 70.2 CAB Net [23] 78.8 73.8 67.3 80.5 85.4 89.5 63.5 88.9 70.7 66.8 83.5 79.4 81.0 72.9 CAB-s Net [23] 78.4 71.2 67.0 83.3 82.2 89.2 64.0 88.2 57.2 75.2 80.1 66.6 87.5 70.7	Faster R-CNN [5]		•					1	1						1
FPN [29] 71.6 79.2 39.1 78.2 58.0 36.5 87.5 85.5 55.7 55.6 71.5 77.3 60.8 58.7 Mask R-CNN [6] 78.5 78.9 48.3 88.5 63.9 58.1 86.7 82.4 58.6 53.3 68.2 76.4 63.5 56.6 SSD512 [7] 66.5 74.9 63.9 84.2 62.1 51.2 85.1 84.2 45.4 66.6 65.7 60.5 58.3 64.0 DSSD512 [30] 56.1 79.6 55.4 85.8 60.7 88.6 79.1 69.6 65.3 68.3 68.2 61.5 65.5 64.7 RFB Net 512 [31] 69.0 77.6 68.8 88.9 67.6 63.0 88.8 84.9 66.8 71.8 71.6 75.0 62.9 70.4 CAB Net [23] 74.7 84.5 82.5 87.5 71.8 64.4 88.4 87.9 68.6 73.3 74.8 79.3 75.1 76.3 CAB-s Net [23] 76.8 85.4 78.0 86.4 71.7 62.3 89.2 88.7 71.5 73.5 75.3 75.9 73.1 75.9 EMDFNet(ours) 88.0 93.6 82.9 94.9 63.2 88.8 92.5 91.6 78.0 80.0 85.0 89.2 84.1 75.3		65.4	74.9	39.1	78.2	58.0	36.5	77.6	74.6	40.5	48.5	60.2	65.4	49.0	51.2
SSD512 [7] 66.5 74.9 63.9 84.2 62.1 51.2 85.1 84.2 45.4 66.6 65.7 60.5 58.3 64.0 DSSD512 [30] 56.1 79.6 55.4 85.8 60.7 88.6 79.1 69.6 65.3 68.3 68.2 61.5 65.5 64.7 RFB Net 512 [31] 69.0 77.6 68.8 88.9 67.6 63.0 88.8 84.9 66.8 71.8 71.6 75.0 62.9 70.4 ScratchDet [18] 71.2 87.3 65.4 79.1 66.8 55.7 85.8 84.7 63.6 67.1 73.2 65.4 69.9 72.8 CAB Net [23] 74.7 84.5 82.5 87.5 71.8 64.4 88.4 87.9 68.6 73.3 74.8 79.3 75.1 76.3 CAB-s Net [23] 76.8 85.4 78.0 86.4 71.7 62.3 89.2 88.7 71.5 73.5 75.3 75.9 73.1 75.9 EMDFNet(ours) 88.0 93.6 82.9 94.9 63.2 88.8 92.5 91.6 78.0 80.0 85.0 89.2 84.1 75.3 Method pl80 pm20 pm30 pm55 pn pne po pm po po pm40 pr40 w13 w55 w57 w59 p27 pl70 pl70 ps3.0 39.0 48.0 39.0 79.0 61.0	FPN [29]	71.6	79.2	39.1	78.2	58.0	36.5	87.5		55.7	55.6	71.5	77.3	60.8	58.7
DSSD512 [30] 56.1 79.6 55.4 85.8 60.7 88.6 79.1 69.6 65.3 68.3 68.2 61.5 65.5 64.7 RFB Net 512 [31] 69.0 77.6 68.8 88.9 67.6 63.0 88.8 84.9 66.8 71.8 71.6 75.0 62.9 70.4 ScratchDet [18] 71.2 87.3 65.4 79.1 66.8 55.7 85.8 84.7 63.6 67.1 73.2 65.4 69.9 72.8 CAB Net [23] 74.7 84.5 82.5 87.5 71.8 64.4 88.4 87.9 68.6 73.3 74.8 79.3 75.1 76.3 CAB-s Net [23] 76.8 85.4 78.0 86.4 71.7 62.3 89.2 88.7 71.5 73.5 75.3 75.9 73.1 75.9 EMDFNet(ours) 88.0 93.6 82.9 94.9 63.2 88.8 92.5 91.6 78.0 80.0 85.0 89.2 84.1 75.3 Method pl80 pm20 pm30 pm55 pn pne po pr40 w13 w55 w57 w59 p27 pl70 pl70 Faster R-CNN [5] 52.0 61.0 67.0 61.0 37.0 47.0 37.0 75.0 33.0 39.0 48.0 39.0 79.0 61.0 Faster R-CNN [6] 71.5 58.0	Mask R-CNN [6]	78.5	78.9	48.3	88.5	63.9	58.1	86.7	82.4	58.6	53.3	68.2	76.4	63.5	56.6
RFB Net 512 [31] 69.0 77.6 68.8 88.9 67.6 63.0 88.8 84.9 66.8 71.8 71.6 75.0 62.9 70.4 ScratchDet [18] 71.2 87.3 65.4 79.1 66.8 55.7 85.8 84.7 63.6 67.1 73.2 65.4 69.9 72.8 CAB Net [23] 74.7 84.5 82.5 87.5 71.8 64.4 88.4 87.9 68.6 73.3 74.8 79.3 75.1 76.3 CAB-s Net [23] 76.8 85.4 78.0 86.4 71.7 62.3 89.2 88.7 71.5 73.5 75.3 75.9 73.1 75.9 EMDFNet(ours) 88.0 93.6 82.9 94.9 63.2 88.8 92.5 91.6 78.0 80.0 85.0 89.2 84.1 75.3 Method pl80 pm20 pm30 pm55 pn pne po pr40 w13 w55 w57 w59 p27 pl70 pl70 Faster R-CNN [5] 52.0 61.0 67.0 61.0 37.0 47.0 37.0 75.0 33.0 39.0 48.0 39.0 79.0 61.0 Faster R-CNN [6] 70.9 55.5 40.1 75.7 89.0 89.8 60.2 87.6 45.3 65.9 70.3 62.3 84.8 63.5	SSD512 [7]	66.5	74.9	63.9	84.2	62.1	51.2	85.1	84.2	45.4	66.6	65.7	60.5	58.3	64.0
ScratchDet [18] 71.2 87.3 65.4 79.1 66.8 55.7 85.8 84.7 63.6 67.1 73.2 65.4 69.9 72.8 CAB Net [23] 74.7 84.5 82.5 87.5 71.8 64.4 88.4 87.9 68.6 73.3 74.8 79.3 75.1 76.3 CAB-s Net [23] 76.8 85.4 78.0 86.4 71.7 62.3 89.2 88.7 71.5 73.5 75.3 75.9 73.1 75.9 EMDFNet(ours) 88.0 93.6 82.9 94.9 63.2 88.8 92.5 91.6 78.0 80.0 85.0 89.2 84.1 75.3 Method pl80 pm20 pm30 pm55 pn pne po pr40 w13 w55 w57 w59 p27 pl70 pl70 Faster R-CNN [5] 52.0 61.0 67.0 61.0 37.0 47.0 37.0 75.0 33.0 39.0 48.0 39.0 79.0 61.0 Faster R-CNN [28] 59.0 50.5 29.1 68.5 77.8 87.5 47.7 86.9 30.9 62.1 67.0 57.2 64.3 61.2 FPN [29] 70.9 55.5 40.1 75.7 89.0 89.8 60.2 87.6 45.3 65.9 70.3 62.3 84.8 63.5 Mask R-CNN [6] 71.5 58.0 41.5 68.8 88.6 90.5 63.0 </td <td>DSSD512 [30]</td> <td>56.1</td> <td>79.6</td> <td>55.4</td> <td>85.8</td> <td>60.7</td> <td>88.6</td> <td>79.1</td> <td>69.6</td> <td>65.3</td> <td>68.3</td> <td>68.2</td> <td>61.5</td> <td>65.5</td> <td>64.7</td>	DSSD512 [30]	56.1	79.6	55.4	85.8	60.7	88.6	79.1	69.6	65.3	68.3	68.2	61.5	65.5	64.7
CAB Net [23] 74.7 84.5 82.5 87.5 71.8 64.4 88.4 87.9 68.6 73.3 74.8 79.3 75.1 76.3 CAB-s Net [23] 76.8 85.4 78.0 86.4 71.7 62.3 89.2 88.7 71.5 73.5 75.3 75.9 73.1 75.9 EMDFNet(ours) 88.0 93.6 82.9 94.9 63.2 88.8 92.5 91.6 78.0 80.0 85.0 89.2 84.1 75.3 Method pl80 pm20 pm30 pm55 pn pne pn pne po pr40 w13 w55 w57 w59 p27 pl70 pl70 Faster R-CNN [5] 52.0 61.0 67.0 61.0 37.0 47.0 37.0 75.0 33.0 39.0 48.0 39.0 79.0 61.0 Faster R-CNN [28] 59.0 50.5 29.1 68.5 77.8 87.5 47.7 86.9 30.9 62.1 67.0 57.2 64.3 61.2 FPN [29] 70.9 55.5 40.1 75.7 89.0 89.8 60.2 87.6 45.3 65.9 70.3 62.3 84.8 63.5 Mask R-CNN [6] 71.5 58.0 41.5 68.8 88.6 90.5 63.0 87.5 51.3 66.6 71.1 61.8 87.5 66.3 SDSD512 [7] 70.5 69.6	RFB Net 512 [31]	69.0	77.6	68.8	88.9	67.6	63.0	88.8	84.9	66.8	71.8	71.6	75.0	62.9	70.4
CAB-s Net [23] 76.8 85.4 78.0 86.4 71.7 62.3 89.2 88.7 71.5 73.5 75.3 75.9 73.1 75.9 EMDFNet(ours) 88.0 93.6 82.9 94.9 63.2 88.8 92.5 91.6 78.0 80.0 85.0 89.2 84.1 75.3 Method pl80 pm20 pm30 pm55 pn pne paster R-CNN [5] 52.0 61.0 67.0 61.0 37.0 47.0 37.0 75.0 33.0 39.0 48.0 39.0 79.0 61.0 37.0 47.0 37.0 75.0 33.0 39.0 48.0 39.0 79.0 61.0 61.0 37.0 47.0 37.0 75.0 33.0 39.0 48.0 39.0 79.0 61.0 61.0 37.0 47.0 37.0 47.0 37.0 75.0 33.0 39.0 48.0 39.0 79.0 61.0 61.0 37.0 47.0 37.0 47.0 37.0 75.0 33.0 39.0 48.0 39.0 79.0 61.0 61.0 37.0 47.0 37.0 47.0 37.0 75.0 33.0 39.0 48.0 39.0 79.0 61.0 61.0 37.0 47.0 37.0 47.0 37.0 47.0 37.0 47.0 37.0 47.0 37.0 47.0 37.0 47.0 37.0 47.0 37.0 47.0 37.0 47.0 37.0 47.0 37.0 47.0 47.0 47.0 47.0 47.0 47.0 47.0 4	ScratchDet [18]	71.2	87.3	65.4	79.1	66.8	55.7	85.8	84.7	63.6	67.1	73.2	65.4	69.9	72.8
EMDFNet(ours) 88.0 93.6 82.9 94.9 63.2 88.8 92.5 91.6 78.0 80.0 85.0 89.2 84.1 75.3 Method pl80 pm20 pm30 pm55 pn pne po pr40 w13 w55 w57 w59 p27 pl70 pl70 pl70 pl70 pl70 pl70 pl70 pl70 pl70	CAB Net [23]	74.7	84.5	82.5	87.5	71.8	64.4	88.4	87.9	68.6	73.3	74.8	79.3	75.1	76.3
Method pl80 pm20 pm30 pm55 pn pne po pr40 w13 w55 w57 w59 p27 pl70 pl70 pl70 pl70 Faster R-CNN [5] 52.0 61.0 67.0 61.0 37.0 47.0 37.0 75.0 33.0 39.0 48.0 39.0 79.0 61.0 pl70 pl70 pl70 pl70 pl70 pl70 pl70 pl7	CAB-s Net [23]	76.8	85.4	78.0	86.4	71.7	62.3	89.2	88.7	71.5	73.5	75.3	75.9	73.1	75.9
Faster R-CNN [5] 52.0 61.0 67.0 61.0 37.0 47.0 37.0 75.0 33.0 39.0 48.0 39.0 79.0 61.0 Faster R-CNN [28] 59.0 50.5 29.1 68.5 77.8 87.5 47.7 86.9 30.9 62.1 67.0 57.2 64.3 61.2 FPN [29] 70.9 55.5 40.1 75.7 89.0 89.8 60.2 87.6 45.3 65.9 70.3 62.3 84.8 63.5 Mask R-CNN [6] 71.5 58.0 41.5 68.8 88.6 90.5 63.0 87.5 51.3 66.6 71.1 61.8 87.5 66.3 SSD512 [7] 70.5 69.6 51.3 71.2 71.7 86.4 51.8 87.9 46.1 64.6 74.0 58.8 76.2 70.6 DSSD512 [30] 75.6 66.3 50.6 76.5 67.2 88.9 51.7 88.0 60.6 70.1 83.6 75.1 60.9 71.0 RFB Net 512 [31] 71.9 73.7 54.0 86.5 78.0 88.2 59.8 84.5 64.8 72.4 81.5 69.3 79.8 64.9 ScratchDet [18] 75.9 73.3 52.2 76.5 76.7 89.4 62.9 85.0 69.1 70.3 84.7 76.5 79.7 70.2 CAB Net [23] 78.8 73.8 67.3 80.5 85.4 89.5 63.5 88.9 70.7 66.8 83.5 79.4 81.0 72.9 CAB-s Net [23] 78.4 71.2 67.0 83.3 82.2 89.2 64.0 88.2 57.2 75.2 80.1 66.6 87.5 70.7	EMDFNet(ours)	88.0	93.6	82.9	94.9	63.2	88.8	92.5	91.6	78.0	80.0	85.0	89.2	84.1	75.3
Faster R-CNN [5] 52.0 61.0 67.0 61.0 37.0 47.0 37.0 75.0 33.0 39.0 48.0 39.0 79.0 61.0 Faster R-CNN [28] 59.0 50.5 29.1 68.5 77.8 87.5 47.7 86.9 30.9 62.1 67.0 57.2 64.3 61.2 FPN [29] 70.9 55.5 40.1 75.7 89.0 89.8 60.2 87.6 45.3 65.9 70.3 62.3 84.8 63.5 Mask R-CNN [6] 71.5 58.0 41.5 68.8 88.6 90.5 63.0 87.5 51.3 66.6 71.1 61.8 87.5 66.3 SSD512 [7] 70.5 69.6 51.3 71.2 71.7 86.4 51.8 87.9 46.1 64.6 74.0 58.8 76.2 70.6 DSSD512 [30] 75.6 66.3 50.6 76.5 67.2 88.9 51.7 88.0 60.6 70.1 83.6 75.1 60.9 71.0 RFB Net 512 [31] 71.9 73.7 54.0 86.5 78.0 88.2 59.8 84.5 64.8 72.4 81.5 69.3 79.8 64.9 ScratchDet [18] 75.9 73.3 52.2 76.5 76.7 89.4 62.9 85.0 69.1 70.3 84.7 76.5 79.7 70.2 CAB Net [23] 78.8 73.8 67.3 80.5 85.4 89.5 63.5 88.9 70.7 66.8 83.5 79.4 81.0 72.9 CAB-s Net [23] 78.4 71.2 67.0 83.3 82.2 89.2 64.0 88.2 57.2 75.2 80.1 66.6 87.5 70.7	Method	p180	pm20	pm30	pm55	pn	pne	ро	pr40	w13	w55	w57	w59	p27	pl70
Faster R-CNN [28] 59.0 50.5 29.1 68.5 77.8 87.5 47.7 86.9 30.9 62.1 67.0 57.2 64.3 61.2 FPN [29] 70.9 55.5 40.1 75.7 89.0 89.8 60.2 87.6 45.3 65.9 70.3 62.3 84.8 63.5 Mask R-CNN [6] 71.5 58.0 41.5 68.8 88.6 90.5 63.0 87.5 51.3 66.6 71.1 61.8 87.5 66.3 SSD512 [7] 70.5 69.6 51.3 71.2 71.7 86.4 51.8 87.9 46.1 64.6 74.0 58.8 76.2 70.2 DSSD512 [30] 75.6 66.3 50.6 76.5 67.2 88.9 51.7 88.0 60.6 70.1 83.6 75.1 60.9 71.0 RFB Net 512 [31] 71.9 73.7 54.0 86.5 78.0 88.2 59.8 84.5 64.8 72.4 81.5 69.3 79.8 64.9 ScratchDet [18] 75.9 73.3 52.2 76.5 76.7 89.4 62.9 85.0 69.1 70.3 84.7 76.5 79.7 70.2 CAB s Net [23] 78.4 71.2 67.0 83.3 82.2 89.2 64.0 88.2 57.2 75.2 80.1 66.6 87.5 70.7	Faster R-CNN [5]	52.0	61.0	67.0	61.0	37.0	47.0	37.0	75.0	33.0	39.0	48.0	39.0	79.0	61.0
Mask R-CNN [6] 71.5 58.0 41.5 68.8 88.6 90.5 63.0 87.5 51.3 66.6 71.1 61.8 87.5 66.3 SSD512 [7] 70.5 69.6 51.3 71.2 71.7 86.4 51.8 87.9 46.1 64.6 74.0 58.8 76.2 70.6 DSSD512 [30] 75.6 66.3 50.6 76.5 67.2 88.9 51.7 88.0 60.6 70.1 83.6 75.1 60.9 71.0 RFB Net 512 [31] 71.9 73.7 54.0 86.5 78.0 88.2 59.8 84.5 64.8 72.4 81.5 69.3 79.8 64.9 ScratchDet [18] 75.9 73.3 52.2 76.5 76.7 89.4 62.9 85.0 69.1 70.3 84.7 76.5 79.7 70.2 CAB Net [23] 78.4 71.2 67.0 83.3 82.2 89.2 64.0 88.2 57.2 75.2 80.1 66.6 87.5 70.7	Faster R-CNN [28]	59.0	50.5	29.1	68.5	77.8	87.5	47.7	86.9	30.9	62.1	67.0	57.2	64.3	61.2
SSD512 [7] 70.5 69.6 51.3 71.2 71.7 86.4 51.8 87.9 46.1 64.6 74.0 58.8 76.2 70.6 DSSD512 [30] 75.6 66.3 50.6 76.5 67.2 88.9 51.7 88.0 60.6 70.1 83.6 75.1 60.9 71.0 RFB Net 512 [31] 71.9 73.7 54.0 86.5 78.0 88.2 59.8 84.5 64.8 72.4 81.5 69.3 79.8 64.9 ScratchDet [18] 75.9 73.3 52.2 76.5 76.7 89.4 62.9 85.0 69.1 70.3 84.7 76.5 79.7 70.2 CAB Net [23] 78.8 73.8 67.3 80.5 85.4 89.5 63.5 88.9 70.7 66.8 83.5 79.4 81.0 72.9 CAB-s Net [23] 78.4 71.2 67.0 83.3 82.2 89.2 64.0 88.2 57.2 75.2 80.1 66.6 87.5 70.7	FPN [29]	70.9	55.5	40.1	75.7	89.0	89.8	60.2	87.6	45.3	65.9	70.3	62.3	84.8	63.5
DSSD512 [30]	Mask R-CNN [6]	71.5	58.0	41.5	68.8	88.6	90.5	63.0	87.5	51.3	66.6	71.1	61.8	87.5	66.3
RFB Net 512 [31] 71.9 73.7 54.0 86.5 78.0 88.2 59.8 84.5 64.8 72.4 81.5 69.3 79.8 64.9 ScratchDet [18] 75.9 73.3 52.2 76.5 76.7 89.4 62.9 85.0 69.1 70.3 84.7 76.5 79.7 70.2 CAB Net [23] 78.8 73.8 67.3 80.5 85.4 89.5 63.5 88.9 70.7 66.8 83.5 79.4 81.0 72.9 CAB-s Net [23] 78.4 71.2 67.0 83.3 82.2 89.2 64.0 88.2 57.2 75.2 80.1 66.6 87.5 70.7	SSD512 [7]	70.5	69.6	51.3	71.2	71.7	86.4	51.8	87.9	46.1	64.6	74.0	58.8	76.2	70.6
ScratchDet [18] 75.9 73.3 52.2 76.5 76.7 89.4 62.9 85.0 69.1 70.3 84.7 76.5 79.7 70.2 CAB Net [23] 78.8 73.8 67.3 80.5 85.4 89.5 63.5 88.9 70.7 66.8 83.5 79.4 81.0 72.9 CAB-s Net [23] 78.4 71.2 67.0 83.3 82.2 89.2 64.0 88.2 57.2 75.2 80.1 66.6 87.5 70.7	DSSD512 [30]	75.6	66.3	50.6	76.5	67.2	88.9	51.7	88.0	60.6	70.1	83.6	75.1	60.9	71.0
CAB Net [23] 78.8 73.8 67.3 80.5 85.4 89.5 63.5 88.9 70.7 66.8 83.5 79.4 81.0 72.9 CAB-s Net [23] 78.4 71.2 67.0 83.3 82.2 89.2 64.0 88.2 57.2 75.2 80.1 66.6 87.5 70.7	RFB Net 512 [31]	71.9	73.7	54.0	86.5	78.0	88.2	59.8	84.5	64.8	72.4	81.5	69.3	79.8	64.9
CAB-s Net [23] 78.4 71.2 67.0 83.3 82.2 89.2 64.0 88.2 57.2 75.2 80.1 66.6 87.5 70.7	ScratchDet [18]	75.9	73.3	52.2	76.5	76.7	89.4	62.9	85.0	69.1	70.3	84.7	76.5	79.7	70.2
	CAB Net [23]	78.8	73.8	67.3	80.5	85.4	89.5	63.5	88.9	70.7	66.8	83.5	79.4	81.0	72.9
EMDFNet(ours) 80.5 79.5 60.3 83.5 96.3 96.6 80.7 92.7 92.7 80.9 87.8 87.9 100.0 72.0	CAB-s Net [23]	78.4	71.2	67.0	83.3	82.2	89.2	64.0	88.2	57.2	75.2	80.1	66.6	87.5	70.7
	EMDFNet(ours)	80.5	79.5	60.3	83.5	96.3	96.6	80.7	92.7	92.7	80.9	87.8	87.9	100.0	72.0

4.5 Qualitative Analysis

To demonstrate the effectiveness of EMDFNet in small object detection, we conduct visualization experiments on the TT100K testing set, as illustrated in Fig. 5.

As shown in the second line of the Fig.5, there are a total of six ground truth objects in the images. MDNet successfully detects all six objects and correctly classifies them with high confidence scores. This can be attributed to the good performance of MDNet

Table 3: The performance of different models on the GTSDB dataset.

Model	mAP@.5	FPS	Params	GFLOPS
SSD Mobilenet [7]	61.6	66.0	5.5	2.3
SSD Inception V2 [7]	66.1	42.1	13.4	7.5
Cascade R-CNN [17]	70.4	-	-	-
Faster R-CNN + IFA-FPN [32]	78.0	-	-	-
YOLO V2 [33]	78.8	46.5	50.5	62.7
Cascade R-CNN + IFA-FPN [32]	80.3	-	-	-
Faster R-CNN Inception V2 [5]	90.6	17.0	12.8	120.6
Faster R-CNN ResNet 50 [5]	91.5	9.6	43.3	533.5
Faster R-CNN ResNet 101 [5]	95.0	8.1	62.3	625.7
R-FCN ResNet 101	95.1	11.7	64.5	269.9
Faster R-CNN Inception ResNet V2 [5]	95.7	2.2	59.4	1837.5
EMDFNet(ours)	97.0	16.7	29.7	190.4

in detecting small objects, demonstrating its robustness and high stability in small traffic sign detection. In contrast, YOLOX only detects two of them and Mask R-CNN only detects four of them. More dramatically, the detected objects 'p19' and 'w55' by YOLOX are completely different from the ground truth objects 'p5' and 'w57'. This discrepancy may be attributed to that the objects are relatively distant and small in the images, resulting in poor classification and detection performance. Results framed in red highlight EMDFNet's ability to accurately detect and classify small, distant, or edge-located signs with high confidence, addressing YOLOX and Mask R-CNN limitations in edge detection and small object classification.

4.6 Ablation Study

To investigate the performance of various components of our EMDFNet, we add the separate component to the baseline to observe the detection performance. All experiments are performed on the TT100K dataset. The ablation results about ASM, EHE, SIoU and Res2net are illustrated in Table 5.

Impact of Augmented Shortcut Module. we first verify ASM's feature diversity capability. As observed in Table 5, mAP@.5 increase by 0.9%, mAP@.75 increase by 1.5%, and mAP@.5:.95 increase by 1.4%. The results show that the mAP value comprehensively improves, proving the ability of ASM feature diversity. ASM enhances input feature diversity beyond standard shortcuts by introducing a transformative multiple branches.

Impact of Efficient Hybrid Encoder. To preserve crucial discriminative information and enhance feature fusion during aggregation and path selection, we integrate EMDFNet's EHE into YOLOX, resulting in significant improvements across various metrics. According to experimental in Table 5, AP_s , AP_m , and AP_l comprehensively enhance. The increase in AP_s , AP_m , and AP_l are 2.0%, 1.5%, and 3.5%, respectively. Therefore, EHE has a very good effect on the fusion of small, medium and large targets. Impact of SIoU. To verify the impact of different loss functions, we conduct ablation experiments on the original IoU Loss and SIoU Loss. EMDFNet's SIoU Loss considers

spatial distances and angles between predicted and actual bounding boxes, improving training efficiency compared to YOLOX's traditional IoU Loss. Experimental results in Table 5 confirm these improvements, enhancing metrics such as mAP@.5, mAP@.75, and mAP@.5:.95, without adding complexity. Notably, mAP@.5 increases by 1.2% to 81.8%.

Table 4: Detection error distribution of YOLOX and EMDFNet on the TT100K testing set. TIDE categorizes errors into six types: Cls (correct localization but incorrect classification), Loc (correct classification but incorrect classification and localization), Dupe detection (correct classification and localization with a prior matching detection), Bkg (detected background as foreground), and Miss (undetected ground truths outside of classification or localization errors).

Model	Cls	Loc	Both	Dupe	Bkg	Miss	FalsePos(FP)	FalseNeg(FN)
YOLOX	11.22	0.44	0.01	0.05	2.71	1.87	7.90	9.67
EMDFNet(ours)	10.02	0.31	0.03	0.08	2.63	0.98	7.47	7.62

Impact of Res2Net. Finally, we assess EMDFNet's Res2Net backbone, which enhances multi-scale features and expands the receptive field of per layer compared to YOLOX's Darknet53. Theoretically, Res2Net offers superior feature extraction, leading to enhanced detection performance. By partitioning input features into different groups and processing them through varying numbers of convolutional blocks, Res2Net achieves multi-scale effect, which is particularly advantageous for small object detection. Experimental results in Table 5 demonstrate improvements across all metrics, with mAP@.5, mAP@.75, mAP@.5:.95, AP_s , AP_m , and AP_l increasing by 1.9%, 2.0%, 2.0%, 0.9%, 2.3%, and 3.6%, respectively. These enhancements, achieving with minimal increase in parameters and computational complexity, affirm the efficacy of Res2Net in EMDFNet.

5 Conclusion

This paper proposes a novel detector EMDFNet to address the issues of feature singularity and weak multi-scale fusion capability. EMDFNet consists of two key components: an Augmented Shortcut Module and an Efficient Hybrid Encoder. The Augmented Shortcut Module utilizes extracted features as input for different branches, conducts various feature selection operations, and ultimately combines them to enhance feature diversity. The Efficient Hybrid Encoder performs information interaction based on intra-scale feature interaction and cross-scale feature fusion. Extensive experiments on challenging datasets such as TT100K and GTSDB demonstrate that our EMDFNet achieves state-of-the-art performance. We will continue to explore lightweight network to better apply them in autonomous driving.

Table 5: Ablation Experiment on the TT100K Dataset. We conduct ablation experiments on ASM, EHE, SIoU and Res2Net.

Model	mAP@.5	mAP@.75	mAP@.5:.95	AP_s	AP_m	$\overline{AP_l}$
YOLOX [34]	80.6	72.8	61.2	53.1	66.1	72.4
YOLOX+ASM	81.5	74.3	62.6	52.7	67.8	73.0
YOLOX+EHE	82.2	74.6	63.1	55.1	67.6	75.9
YOLOX+SIoU	81.8	73.0	61.7	53.4	66.6	71.2
YOLOX+Res2Net	82.5	74.8	63.2	54.0	68.4	76.0
EMDFNet(ours)	84.4	76.8	64.9	55.4	68.5	81.7



Fig. 5: Comparison of detection performance between EMDFNet and other models on the TT100K testing set. Zoom in to see details.

References

- M. Everingham, L. Van Gool, C. K. Williams, J. Winn, and A. Zisserman, "The pascal visual object classes (voc) challenge," *International journal of computer vision*, vol. 88, pp. 303– 338, 2010.
- T.-Y. Lin, M. Maire, S. Belongie, J. Hays, P. Perona, D. Ramanan, P. Dollár, and C. L. Zitnick, "Microsoft coco: Common objects in context," in *Computer Vision–ECCV 2014: 13th European Conference, Zurich, Switzerland, September 6-12, 2014, Proceedings, Part V 13.* Springer, 2014, pp. 740–755.
- 3. R. Girshick, J. Donahue, T. Darrell, and J. Malik, "Rich feature hierarchies for accurate object detection and semantic segmentation," in *Proceedings of the IEEE conference on computer vision and pattern recognition*, 2014, pp. 580–587.
- 4. R. Girshick, "Fast r-cnn," in *Proceedings of the IEEE international conference on computer vision*, 2015, pp. 1440–1448.
- S. Ren, K. He, R. Girshick, and J. Sun, "Faster r-cnn: Towards real-time object detection with region proposal networks," *Advances in neural information processing systems*, vol. 28, 2015.
- 6. K. He, G. Gkioxari, P. Dollár, and R. Girshick, "Mask r-cnn," in *Proceedings of the IEEE international conference on computer vision*, 2017, pp. 2961–2969.
- W. Liu, D. Anguelov, D. Erhan, C. Szegedy, S. Reed, C.-Y. Fu, and A. C. Berg, "Ssd: Single shot multibox detector," in *Computer Vision–ECCV 2016: 14th European Conference, Am*sterdam, The Netherlands, October 11–14, 2016, Proceedings, Part I 14. Springer, 2016, pp. 21–37.
- 8. Y. Zhu, C. Zhang, D. Zhou, X. Wang, X. Bai, and W. Liu, "Traffic sign detection and recognition using fully convolutional network guided proposals," *Neurocomputing*, vol. 214, pp. 758–766, 2016.
- 9. S.-H. Gao, M.-M. Cheng, K. Zhao, X.-Y. Zhang, M.-H. Yang, and P. Torr, "Res2net: A new multi-scale backbone architecture," *IEEE transactions on pattern analysis and machine intelligence*, vol. 43, no. 2, pp. 652–662, 2019.
- D. Ouyang, S. He, G. Zhang, M. Luo, H. Guo, J. Zhan, and Z. Huang, "Efficient multi-scale attention module with cross-spatial learning," in *ICASSP 2023-2023 IEEE International Conference on Acoustics, Speech and Signal Processing (ICASSP)*. IEEE, 2023, pp. 1–5.
- 11. D. Wan, R. Lu, S. Shen, T. Xu, X. Lang, and Z. Ren, "Mixed local channel attention for object detection," *Engineering Applications of Artificial Intelligence*, vol. 123, p. 106442, 2023.
- 12. W. Lv, S. Xu, Y. Zhao, G. Wang, J. Wei, C. Cui, Y. Du, Q. Dang, and Y. Liu, "Detrs beat yolos on real-time object detection," *arXiv preprint arXiv:2304.08069*, 2023.
- 13. Z. Gevorgyan, "Siou loss: More powerful learning for bounding box regression," *arXiv* preprint arXiv:2205.12740, 2022.
- 14. Z. Zhu, D. Liang, S. Zhang, X. Huang, B. Li, and S. Hu, "Traffic-sign detection and classification in the wild," in *Proceedings of the IEEE conference on computer vision and pattern recognition*, 2016, pp. 2110–2118.
- 15. S. Houben, J. Stallkamp, J. Salmen, M. Schlipsing, and C. Igel, "Detection of traffic signs in real-world images: The German Traffic Sign Detection Benchmark," in *International Joint Conference on Neural Networks*, no. 1288, 2013.
- T.-Y. Lin, P. Goyal, R. Girshick, K. He, and P. Dollár, "Focal loss for dense object detection," in *Proceedings of the IEEE international conference on computer vision*, 2017, pp. 2980–2988

- 17. Z. Cai and N. Vasconcelos, "Cascade r-cnn: Delving into high quality object detection," in *Proceedings of the IEEE conference on computer vision and pattern recognition*, 2018, pp. 6154–6162.
- 18. R. Zhu, S. Zhang, X. Wang, L. Wen, H. Shi, L. Bo, and T. Mei, "Scratchdet: Training single-shot object detectors from scratch," in *Proceedings of the IEEE/CVF conference on computer vision and pattern recognition*, 2019, pp. 2268–2277.
- 19. Z. Tian, C. Shen, H. Chen, and T. He, "Fcos: Fully convolutional one-stage object detection," in *Proceedings of the IEEE/CVF international conference on computer vision*, 2019, pp. 9627–9636.
- Z. Liang, J. Shao, D. Zhang, and L. Gao, "Traffic sign detection and recognition based on pyramidal convolutional networks," *Neural Computing and Applications*, vol. 32, pp. 6533– 6543, 2020.
- P. Sun, R. Zhang, Y. Jiang, T. Kong, C. Xu, W. Zhan, M. Tomizuka, L. Li, Z. Yuan, C. Wang et al., "Sparse r-cnn: End-to-end object detection with learnable proposals," in *Proceedings* of the IEEE/CVF conference on computer vision and pattern recognition, 2021, pp. 14454– 14463
- 22. Z. Liu, Y. Lin, Y. Cao, H. Hu, Y. Wei, Z. Zhang, S. Lin, and B. Guo, "Swin transformer: Hierarchical vision transformer using shifted windows," in *Proceedings of the IEEE/CVF international conference on computer vision*, 2021, pp. 10012–10022.
- L. Cui, P. Lv, X. Jiang, Z. Gao, B. Zhou, L. Zhang, L. Shao, and M. Xu, "Context-aware block net for small object detection," *IEEE Transactions on cybernetics*, vol. 52, no. 4, pp. 2300–2313, 2020.
- 24. J. Chu, C. Zhang, M. Yan, H. Zhang, and T. Ge, "Trd-yolo: A real-time, high-performance small traffic sign detection algorithm," *Sensors*, vol. 23, no. 8, 2023.
- 25. Y. Han, F. Wang, W. Wang, X. Li, and J. Zhang, "Yolo-sg: Small traffic signs detection method in complex scene," *The Journal of Supercomputing*, pp. 1–22, 2023.
- Y. Shi, F. Lv, X. Wang, C. Xia, S. Li, S. Yang, T. Xi, and G. Zhang, "Open-transmind: A new baseline and benchmark for 1st foundation model challenge of intelligent transportation," in *Proceedings of the IEEE/CVF Conference on Computer Vision and Pattern Recognition*, 2023, pp. 6327–6334.
- 27. G. Zeng, W. Huang, Y. Wang, X. Wang, and E. Wenjuan, "Transformer fusion and residual learning group classifier loss for long-tailed traffic sign detection," *IEEE Sensors Journal*, pp. 1–1, 2024.
- 28. K. He, X. Zhang, S. Ren, and J. Sun, "Deep residual learning for image recognition," in *Proceedings of the IEEE conference on computer vision and pattern recognition*, 2016, pp. 770–778.
- 29. T.-Y. Lin, P. Dollár, R. Girshick, K. He, B. Hariharan, and S. Belongie, "Feature pyramid networks for object detection," in *Proceedings of the IEEE conference on computer vision and pattern recognition*, 2017, pp. 2117–2125.
- 30. C.-Y. Fu, W. Liu, A. Ranga, A. Tyagi, and A. C. Berg, "Dssd: Deconvolutional single shot detector," *arXiv preprint arXiv:1701.06659*, 2017.
- 31. S. Liu, D. Huang *et al.*, "Receptive field block net for accurate and fast object detection," in *Proceedings of the European conference on computer vision (ECCV)*, 2018, pp. 385–400.
- 32. Q. Tang, G. Cao, and K.-H. Jo, "Integrated feature pyramid network with feature aggregation for traffic sign detection," *IEEE Access*, vol. 9, pp. 117784–117794, 2021.
- 33. J. Redmon and A. Farhadi, "Yolo9000: better, faster, stronger," in *Proceedings of the IEEE conference on computer vision and pattern recognition*, 2017, pp. 7263–7271.
- 34. Z. Ge, S. Liu, F. Wang, Z. Li, and J. Sun, "Yolox: Exceeding yolo series in 2021," arXiv preprint arXiv:2107.08430, 2021.